Stimuli-Responsive Resorcin[4]arene Cavitands: Toward Visible Light-Activated Molecular Grippers

Víctor García-López,*[a] Michal Zalibera,[b] Nils Trapp,[a] Martin Kuss-Petermann,[c] Oliver S. Wenger,[c] François Diederich*[a]

[a] Dr. V. García-López, Dr. N. Trapp, Prof. Dr. F. Diederich
Laboratory of Organic Chemistry, Department of Chemistry and Applied Biosciences
ETH Zurich
HCI, Vladimir-Prelog-Weg 3, 8093, Zurich, Switzerland
E-mail: vicgarcia.chem@gmail.com, diederich@org.chem.ethz.ch

[b] Dr. M. Zalibera
Institute of Physical Chemistry and Chemical Physics
Slovak University of Technology
Radlinského 9, 81237, Bratislava, Slovakia

[c] Dr. M. Kuss-Petermann, Prof. Dr. O. S. Wenger
Department of Chemistry
University of Basel
St. Johanns-Ring 19, 4056, Basel Switzerland

Supporting Information for this article is given via a link at the end of the document

Abstract: Resorcin[4]arene cavitands, equipped with diverse quinone (**Q**) and $[Ru(bpy)_2dppz]^{2+}$ photosensitizing walls in different configurations, were synthesized. Upon visible light irradiation at 420 nm, electron transfer from the $[Ru(bpy)_2dppz]^{2+}$ to the **Q** generates the semiquinone (**SQ**) radical anion, triggering a large conformational switching from a flat *kite* to a *vase* with a cavity for the encapsulation of small guests, such as cyclohexane and heteroalicyclic derivatives, in CD_3CN. Depending on the molecular design, the **SQ** radical anion can live for several minutes (~10 min) and the *vase* can be generated in a secondary process without need for addition of a sacrificial electron donor to accumulate the **SQ** state. Switching can also be triggered by other stimuli, such as changes in solvent, host-guest complexation, and chemical and electrochemical processes. This comprehensive investigation benefits the development of stimuli-responsive nanodevices, such as light-activated molecular grippers.

Introduction

Stimuli-responsive molecules, such as molecular machines[1-14] and switches,[15-18] are molecules that upon stimulation can move their submolecular components in a defined manner to produce a specific function. Molecular grippers are a type of switch that upon stimuli activation can encapsulate or release smaller molecules.[19-21] Such a feature is highly desired for the development of next-generation sensors, receptors, energy conversion devices, and catalysts.

Resorcin[4]arene cavitands are a suitable platform for the development of molecular grippers because they can switch between an open (*kite*) and a closed (*vase*) conformation.[22,23] The former has a large flat surface while the latter features a deep cavity for the encapsulation of small molecules. This *kite-vase* switching has been achieved by changes in temperature[23-26], pH,[27] and solvent,[28,29] metal ion complexation,[30] and by redox reactions[21,31] (Figure 1). However, most of these stimuli require either the addition of chemical fuels that generate waste and deteriorate the system or direct contact between the gripper and an electrode in an electrochemical cell. Light activation is an alternative that allows "wireless" spatiotemporal activation of the system. However, triggering the *kite-vase* switching with light is not trivial.

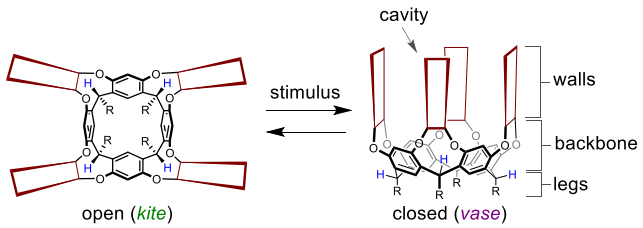

Figure 1. Representation of stimuli-responsive resorcin[4]arene cavitands. The chemical shifts of the methine protons (blue) are used to monitor the conformational change by ^1H NMR spectroscopy.

Different approaches have been used to modulate the encapsulation of molecules by resorcin[4]arene cavitands with light. For instance, Berryman and coworkers designed a cavitand with an azobenzene wall.[32] In the *vase* conformation, the cavitand binds small molecules, but upon irradiation with UV light, the azobenzene moiety adopts the *cis*-isomer which self-fills the cavity and eject the guests out of the cavity. However, this system was predefined in the *vase* conformation and a full *kite-vase* switching was not investigated.

Our group triggered the *kite-vase* switching through an intermolecular photoredox process. The system consisted of a rescorcin[4]arene cavitand with two quinoxaline (Qx) walls and two redox-active quinone (**Q**) walls.[33,34] When the *kite* conformation was irradiated with visible light in the presence of $[Ru(bpy)_3]^{2+}$ (bpy = 2,2'-bipyridine) and triethyl amine (Et_3N), an intermolecular electron transfer from the $[Ru(bpy)_3]^{2+}$ to the **Q** occurred and the corresponding semiquinone radical anions (**SQ**)

were generated. As a secondary process, the switching to the *vase* conformation occurred in the newly formed **SQ** state. The main drawback of this approach is the need of Et_3N, as a sacrificial electron donor, to regenerate the $[Ru(bpy)_3]^{2+}$ and to delay the back-electron transfer reaction from **SQ** until the conformational switching takes place. During this process, side products and chemical waste are accumulated, which could limit the use of the system in energy-converting devices, such as solar cells.[35]

In an attempt to optimize the system, we designed resorcin[4]arene cavitand **1** with two **Q** walls and two Ru^{II}-based photosensitizers ($[Ru(bpy)_2(dppz)]^{2+}$; dppz = dipyrido[3,2-*a*:2',3'-*c*]phenazine) installed directly within the backbone (Figure 2).[36] Upon visible light irradiation (420 nm), intramolecular electron transfer from the Ru^{II}-based walls to the **Q** occurred, forming the **SQ**. Strong steric and electrostatic repulsion between the two bulky Ru^{II}-based walls however prohibited the formation of the *vase*, and only a partial contraction was achieved. Also, this system required the addition of Et_3N as a sacrificial donor.

Here, we report a new series of resorcin[4]arene cavitands armed with single $[Ru(bpy)_2(dppz)]^{2+}$ photosensitizers and different types of **Q**-based walls incorporated in the cavitand backbone in different configurations (Figure 2). Through fine-tuning of the structural design, we developed Ru^{II}-based cavitands that can adopt the *vase* conformation, bind smaller guests, and can be switched from the *kite* to the *vase* upon irradiation with visible light without addition of a sacrificial electron donor. Moreover, the switching can be triggered by other stimuli such as changing the solvent, host-guest interactions, and chemical and electrochemical reactions. Remarkably, not only a large conformational rearrangement is produced upon activation but also a distinctive change of the magnetic and photoluminescence (PL) properties of the system occurs. Thus, in addition to overcoming the limitations of previous resorcin[4]arene cavitands and bringing closer the development of light-activated molecular grippers, the new Ru^{II}-based cavitands are promising candidates for their incorporation as switchable units in multi-stimuli responsive materials and nanodevices.

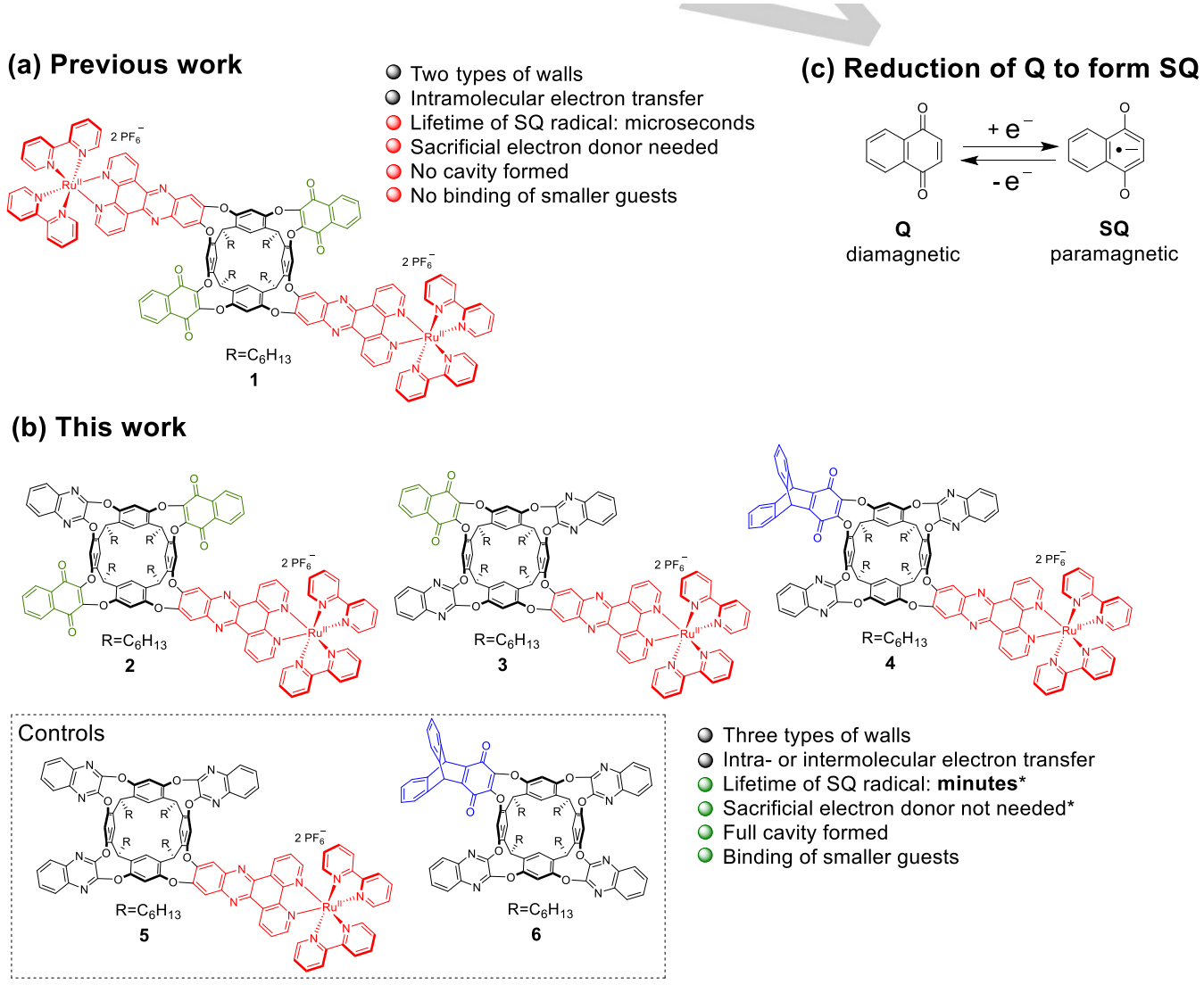

Figure 2. (a), (b) Chemical structures of Ru^{II}-based resorcin[4]arene cavitands **1**-**5** and control **6.** *Only for cavitands **3** and **4.** (c) Redox equilibrium between quinone (**Q**) and semiquinone radical anion (**SQ**).

Results and Discussion

Molecular Design and Synthesis. Previously reported Ru^{II}-based cavitand **1** has three limitations: (1) it is not able to adopt the *vase* conformation because of the steric and electrostatic repulsion between the two Ru^{II}-walls, (2) it cannot bind small guest molecules, and (3) the back-electron transfer occurs in ~3.7 μs competing with the desired slower conformational change occurring in the μs–ms regime.[36] Thus, cavitand **1** requires Et_3N as a sacrificial electron donor to accumulate the **SQ**.

The new Ru^{II}-based cavitands contain only one photosensitizer instead of two to avoid the repulsion that hinders the *vase* formation in **1**, and the position of the **Q** in the backbone was changed to slow down the back-electron transfer. Additionally, quinones (**Q**) with different structural and redox features were incorporated to improve the electron transfer process and the binding of small guests. For instance, cavitand **2** contains one Ru^{II}-based wall, two naphthoquinone **Q** walls in opposite positions, and one unreactive Qx wall. However, in this design, only one of the two **Q** can be reduced to the **SQ** by intramolecular electron transfer from the single Ru^{II}-photosensitizer. This opens the question if a single **SQ** is sufficient to trigger the *kite-vase* switching or whether two **SQ** in opposite positions are required as in previous systems.[33,34] In cavitand **2**, the proximity between the **Q** and the photosensitizer is identical as in **1**. The back-electron transfer is therefore expected to be in the μs regime as well, and Et_3N would be needed to accumulate the **SQ**.

Cavitand **3** features one naphthoquinone **Q** and one Ru^{II}-based wall placed in opposite positions, and the two Qx walls occupy the remaining positions in a cross configuration. The distance between the photosensitizer and the **Q** is larger than in **2**, and a slower back-electron transfer is thus expected. Additionally, the properties of cavitand **3** allowed us to use UV–Vis–NIR spectroelectrochemistry to evaluate if the reduction of a single **Q** is sufficient to induce the *kite-vase* switching.

Cavitand **4** has a configuration similar to **3**, differing by a triptycene-quinone wall (**Q**) that was used instead of the naphthoquinone. We envisioned that the triptycene and the ligands of the Ru^{II}-photosensitizer can cover the top of the cavity, without creating steric repulsions, to provide better gripping and guest-binding properties.[37] Furthermore, the triptycene-quinone is known to have a lower reduction potential than the corresponding naphthoquinone so a more efficient electron transfer is expected in **4** than in **3**.[33]

Cavitands **5** and **6** have three Qx walls and either one **Q** or one Ru^{II}-based wall. These cavitands are designed as controls to explore if both components, the photosensitizer and the electron acceptor **Q**, are required for the light-activation process that forms the **SQ** and triggers the *kite-vase* switching. These controls are important to check whether the **SQ** could be generated by the direct excitation of the **Q** at 420 nm and whether the intended *kite-vase* switching is triggered by a local heating effect caused by the light irradiation or, alternatively, by the non-radiative decay of the Ru^{II}-photosensitizer.

Contrary to cavitand **1** and most resorcin[4]arene cavitands that contain only two types of walls, **2**–**4** feature three different types of walls placed in specific sites of the backbone. Therefore, new synthetic routes were carried out for their synthesis The preparation of **4** is exemplarily shown in Scheme 1. The details for all synthesis are included in the Supporting Information. Through careful purification, validated by structural characterization, cavitands were obtained free of impurities or Ru^{II}-complex residues that could participate in the photoredox process.

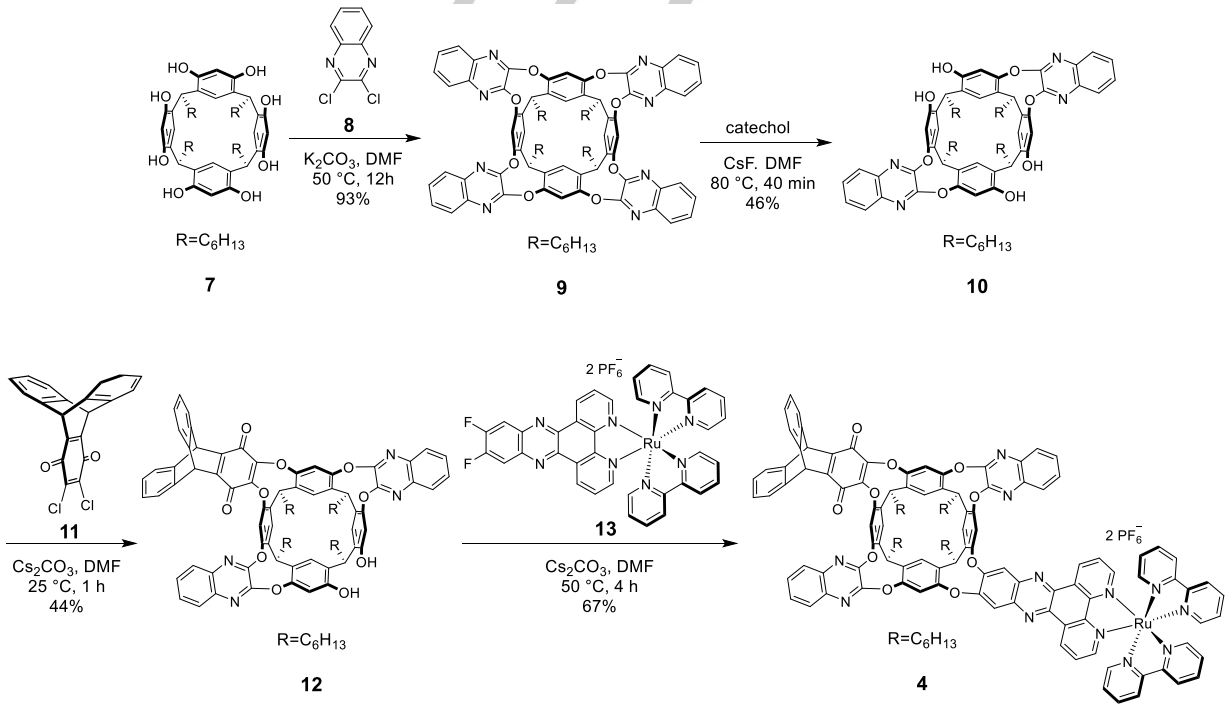

Scheme 1. Synthesis of cavitand **4**.

Probing the Conformation in the Oxidized (Q) State. The conformation of **2**–**6** at room temperature was determined experimentally by ^{1}H NMR spectroscopy in different solvents by monitoring the chemical shifts of the methine protons in the resorcin[4]arene backbone (Figures 1 and S1–S4). Usually, the methine proton signals are detected between 3.4–4.7 ppm in the *kite* and between 5.2–6.0 ppm in the *vase*. We found at 298 K that cavitands **2, 3, 4**, and **6** prefer the *kite* conformation in solvents such as CD_3CN and CD_2Cl_2. Cavitand **2** adopts the *vase* conformation in THF-d_8 but not in DMF-d_7. Contrary was found for **3** and **4** as they adopt the *vase* in DMF-d_7. Cavitand **6** takes on the *vase* form in both THF-d_8 and DMF-d_7. Surprisingly, **5** is in the *vase* conformation in all the solvents used. Thus, it was confirmed that resorcin[4]arene cavitands **2**–**6** can close to the *vase* conformation in solvents that fit in the cavity and stabilize the *vase*, such as DMF or THF.[31,33,37] This is not the case for **1**, which prefers the *kite* conformation in most solvents because of the repulsion between the two Ru^{II}-based walls that hinders the *vase* closure.[36]

Although ^{1}H NMR spectroscopy is useful to follow the conformational change in the **Q** state, the **SQ** radicals are difficult to study by this technique since the interactions with unpaired electrons contribute to the broadening and virtual disappearance of proton resonances. Thus, it was necessary to validate a different technique, namely UV–Vis absorption spectroscopy, to follow the *kite*-*vase* conformational switching in both the **Q** and the **SQ** states. With the precise conformation, confirmed by ^{1}H NMR in different solvents, we looked for distinctive features of the *kite* and the *vase* in the UV–Vis absorption spectra that would allow us to monitor the switching process. Similar to the NMR studies, we measured the absorption spectrum in solvents where the *kite* is preferred and compared it to the spectrum in solvents where the *vase* is formed. All the cavitands show the absorption band at 250–350 nm characteristic for the backbone of resorcin[4]arene cavitands and quinoxalines walls (Qx), but only **2**–**5** have the MLCT absorption band at 390–550 nm characteristic for the $[Ru(bpy)_2(dppz)]^{2+}$ complex (Figure 3 and Figure S5). As an example, Figure 3 shows the spectra of cavitands **4** and **5** in CH_2Cl_2 and DMF. When **4** is in the *vase* conformation (in DMF), the absorption spectrum shows a hypochromic shift at 300–350 nm and 400 nm, and a hyperchromic shift at 350–400 nm when compared to the spectrum in the *kite* conformation (in CH_2Cl_2). Similar shifts in the absorption spectra were observed for **2**, **3**, and **6** when studied in the appropriate solvents (Figure S5). On the other hand, cavitand **5**, which NMR data identify in the *vase* conformation in all the solvents tested, did not show differences in the UV–Vis absorptions among both solvents (DMF and CH_2Cl_2, Figure 3). Moreover, when the UV–Vis absorption spectra of **2**–**5** in CH_2Cl_2 are plotted together, the spectra of **2**–**4** (*kite*) are almost superimposable and the cavitand **5** (*vase*) shows a very different absorption pattern (Figure S6). This confirms that the *kite* and *vase* conformations display distinctive absorptions because of the difference in geometry and not due to a solvent polarity effect.

The photoluminescence (PL) spectra of **2**–**5** were measured in CH_2Cl_2 at identical concentration (Figure S6) and the intensity of PL was found to decrease in the order **5**>**3**>**4**>**2**. Cavitand **5** exhibits the highest PL since it lacks the quinone group that quenches the PL of the Ru^{II}-complex. On the other hand, the PL of cavitand **2** is ~3 times weaker than in **5**, because of the nearby quinones that quench the PL of the Ru^{II}-complex through an intramolecular electron transfer. Because the quinones in **3** and **4** are located at a greater distance from the Ru^{II}-complex than in **2**, the electron transfer is less efficient. The data suggest that the triptycene-quinone in **4** is a better electron acceptor than the naphthoquinone in **3**.

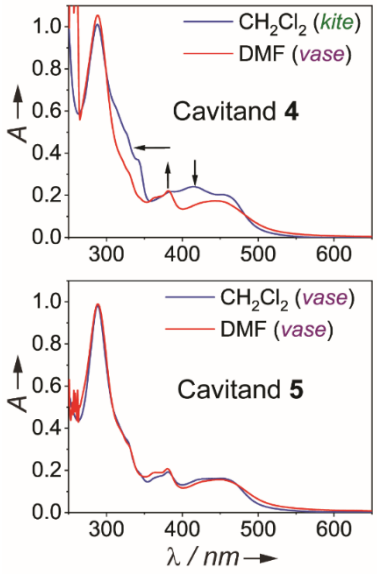

Figure 3. UV–Vis absorption spectra of **4** and **5** (1 x 10^{-5} M) in CH_2Cl_2 and DMF under Ar atmosphere at T = 298 K. The conformational assignments were corroborated by ^{1}H NMR spectroscopy (Supporting Information).

Several attempts to obtain crystal structures of **2**–**6** in both the *kite* and the *vase* conformations were carried out. However, only the crystal structure of **6** in the *vase* form was successfully resolved. When **6** is crystallized from DMF, one molecule of DMF got encapsulated in the cavity and another in the hydrophobic space between the aliphatic legs (Figure 4 and S7). This agrees with the ^{1}H NMR (Figure S4) and UV–Vis absorption (Figure S5) experiments showing the *vase* conformation in DMF. Additionally, the crystal structures of three-wall precursors (cavitands missing the Ru^{II}-based wall) encapsulating a solvent molecule in the *vase* conformation were also obtained (Figures S8–S10).

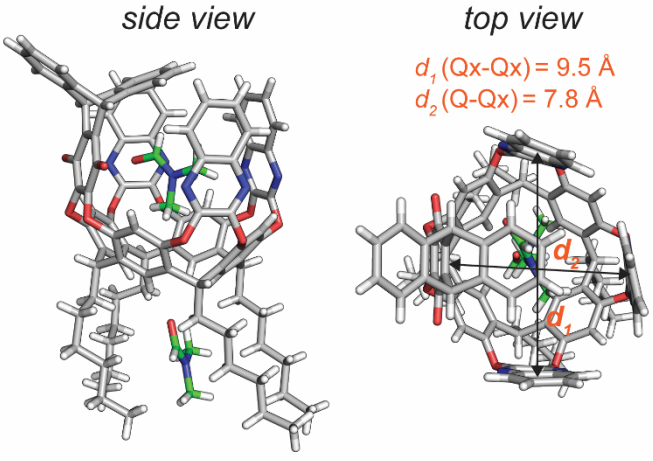

Figure 4. Crystal structure of cavitand **6** in the *vase* conformation crystallized from DMF. Distances: Qx–Qx = 9.5 Å, **Q**–Qx = 7.8 Å.

Since no crystal structures were obtained for **1**–**4**, we carried out DFT B3LYP/6-31G(d) + LANL2DZ level theoretical calculations to visualize the geometry in the **Q** state in both the *kite* and *vase* conformations.[38-40] For all the cavitands, the *kite* conformation consists of a large flat surface, similar to crystal structures of other reported resorcin[4]arene cavitands (Figure S11).[31,37] However, for the gripping function, the evaluation of the geometry and shape of the *vase* conformation is more important. As previously reported, **1** cannot adopt the full *vase* but instead a partially contracted form.[36] On the other hand, as demonstrated experimentally by NMR and UV–Vis absorption spectroscopy, **2**–**4** can adopt the *vase* form. DFT calculations suggest that the *vase* geometry in **2**–**4** is closely similar to **6** observed in the solid-state (Figures 4–5). However, it is important to note that small differences in geometry arise since the calculations neglected the effect of the solvent or the counteranions of the Ru^{II}-complex, while the crystal structure represents the geometry in the solid-state. Nevertheless, the small differences between the *vases* of **2**–**4** predicted by the DFT calculations can explain the experimental data. As intended, the triptycene and the ligands of the Ru^{II}-complex in **4** partially block the top of the cavity which is anticipated to provide better gripping properties.

Gripping Properties, Binding of Cycloalkanes. Having identified the spectroscopic signatures of the *kite* and the *vase*, we studied the binding of typical guest molecules[33] by ^{1}H NMR, UV–Vis, and photoluminescence (PL) spectroscopy. Binding constants were first measured by ^{1}H NMR spectroscopy using CD_3CN as a solvent. Typically, we use mesitylene-d_{12} as a solvent because it is too big to compete with the smaller guests for the cavity binding site, but none of the Ru^{II}-based cavitands are soluble in mesitylene-d_{12}. Thus, we opted to use CD_3CN, a more polar solvent that is too small to stabilize the *vase* or to compete efficiently for the binding site. In pure CD_3CN, cavitand **4** is in the *kite* conformation and upon guest addition, a guest-induced switching to the *vase* conformation was achieved (Figures 6 and S12). The highest binding constant was measured for 1,4-dithiane (K_a = 230 M^{-1}), in agreement with previous triptycene-based cavitands lacking the Ru^{II}-based wall.[29,31] As expected, cavitands **2** and **3** are much less efficient grippers with K_a < 1 for all the guests studied.

Because of the high sensitivity of PL spectroscopy, we were also interested in establishing an approach to measure binding constants with this technique. The rationale is that in **3** and **4**, the **Q** can quench the photoluminescence of the Ru^{II}-complex more efficiently in the *vase* than in the *kite* conformation through an intramolecular electron transfer. Encapsulation of the guest induces the *vase* conformation, bringing the **Q** and the Ru^{II}-complex in proximity for a more efficient PL quenching. Thus, the degree of quenching is proportional to the efficiency of the guest binding and the *vase* formation. The higher binding constants translate to stronger quenching. By treating the process as static quenching and adapting the Stern-Volmer plot, we determined binding constants values in the same order of magnitude to those obtained by ^{1}H NMR (Figure 6 and S13). The experimental details and data analysis are reported in the Supporting Information (Figure S13). UV–Vis absorption spectroscopy was used to provide additional evidence that *kite-vase* switching occurs upon guest encapsulation (Figure S13b).

Chemical and Electrochemical Activation of Resorcin[4]arene Cavitands. The redox properties of cavitands **2**–**6** were investigated in CH_2Cl_2 and in DMF (0.1 M Bu_4NPF_6, using Fc^+/Fc as internal standard) by cyclic voltammetry (CV) and square-wave voltammetry (SWV). The data is shown in Figures S14–S17 and Tables S4–S5. In CH_2Cl_2, cyclic voltammograms of cavitands **2**–**5** showed one reversible one-electron wave between +0.97 V and +1.00 V that corresponds to the oxidation of the Ru^{II} to Ru^{III}.[41] Moreover, several one-electron reductions waves were observed that correspond to the reduction of the dppz ligand (between -1.37 V and -1.42 V) and the bipyridine ligands (between -1.79 V and -2.11 V).[36] The reduction wave of the **Q** to the **SQ** appears at -1.07 V for the naphthoquinone (cavitands **2**, **3**) and between -0.86 and -0.88 V for the triptycene-quinone (cavitands **4**, **6**), confirming the easier reduction of the triptycene-quinone. The reduction wave of the **SQ** to the quinone dianion (Q^{2-}) appears between -1.45 V and -1.54 V in cavitands **2**–**4** and **6**. As expected, the voltammogram of cavitand **5** does not show waves corresponding to the reduction of the **Q** or the **SQ**. Employing DMF as solvent resulted in similar redox potential values although adsorption at the electrode was observed in some cases.

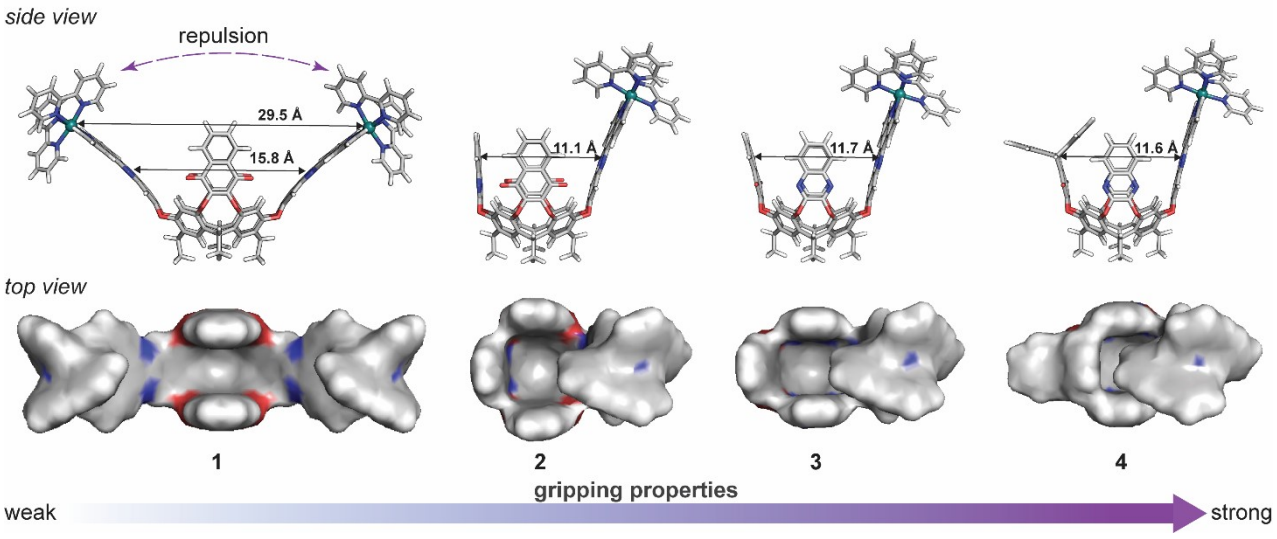

Figure 5. Optimized geometries (DFT B3LYP/6-31G(d) + LANL2DZ) of cavitands **1**–**4** in the vase conformation. Solvent and counterions were not considered during the calculations. For the optimized geometries in the *kite* form, see the Supporting Information.

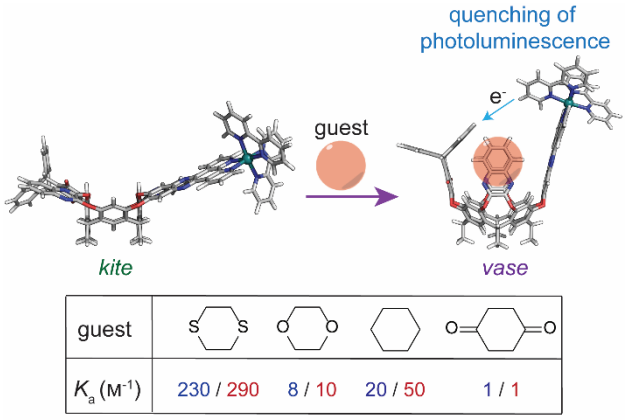

Figure 6. Binding of typical guests by **4** in the **Q** state induces *kite-vase* switching accompanied by PL quenching of the Ru^{II}-complex. Binding constants (K_a) were measured by NMR (blue values; 500 MHz, T = 298 K in CD_3CN) and by PL (red values; T = 298 K in CH_3CN).

EPR/UV–Vis–NIR spectroelectrochemistry (SEC) was employed to monitor the **SQ** formation and the conformational switching upon electrochemical reduction in the potential range of the first reduction step of the **Q** (Figure 7 and Figures S19–S27). The UV–Vis–NIR absorption spectrum of **4** in CH_2Cl_2 upon the one-electron reduction shows hypochromic shifts at 300–350 nm and 400 nm, and an hyperchromic shift at 350–400 nm matching the spectral signature of the *vase* conformation observed in DMF (Figure 7b vs Figure 3 in DMF). Additionally, a new absorption band with a maximum at 445 nm was formed, which according to previously reported cavitands, corresponds to the SOMO-LUMO transitions in the **SQ** radical anion (Figure 7b).[36,42] To better perceive the changes in the absorption spectra, the differential absorption spectrum was plotted confirming the **SQ** formation, which is characterized by the absorption at 400–500 nm (Figure 7c). Furthermore, the absorption changes at 403 nm and 445 nm were monitored during several redox cycles confirming the reversibility of the *kite*(**Q**)–*vase*(**SQ**) switching (Figure 7d). The EPR spectrum of **4** after electrochemical reduction confirmed the formation of the corresponding **SQ**, showing a single line at g = 2.0050 (Figure 7e) with additional unresolved ^{13}C satellite signals.[33] The same set of experiments were carried out for the other cavitands demonstrating the *kite*(**Q**)–*vase*(**SQ**) switching for **2**, **3**, **4**, and **6** upon electrochemical reduction of the corresponding **Q** (Figures S19–S27). No conformational change or **SQ** formation was observed for **5**, demonstrating that the *kite*–*vase* switching can be electrochemically triggered only if the cavitand contains at least one **Q** based wall. The SEC experiments were carried out in deoxygenated solutions of CH_2Cl_2 to avoid the reaction of the **SQ** with oxygen.

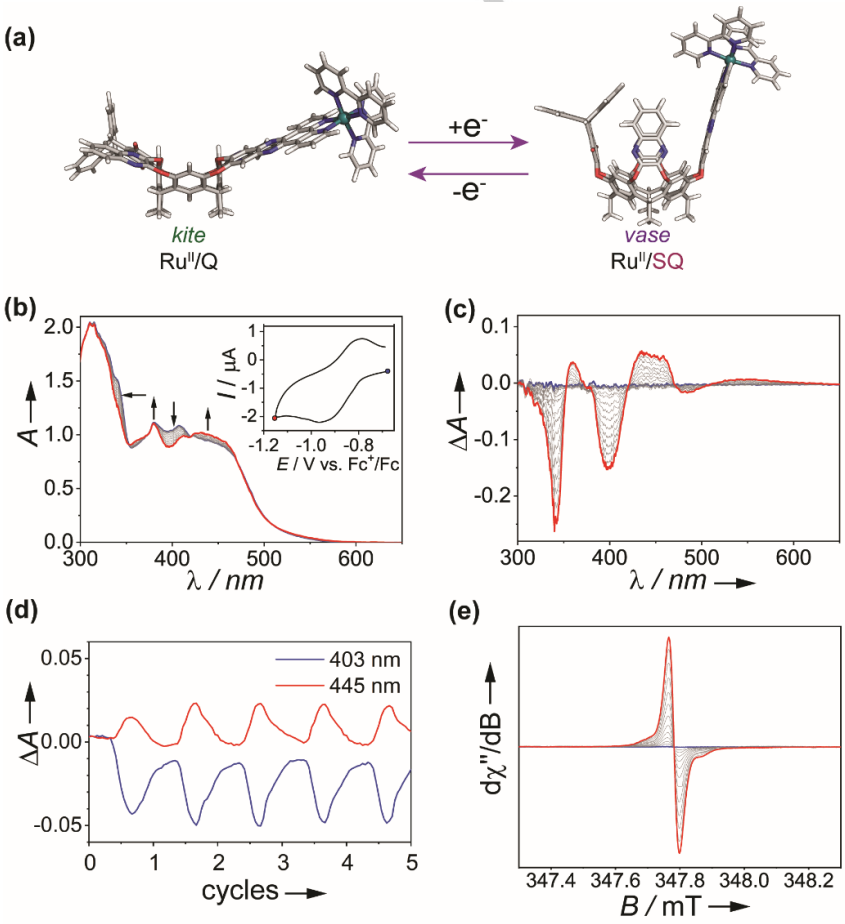

Figure 7. Electrochemical activation of cavitand **4**. (a) Schematic of the switching. (b) UV–Vis–NIR spectroelectrochemistry in the potential region of the first reduction step in 0.2 M n-$(Bu)_4PF_6$/CH_2Cl_2 measured at T = 293 K with a scan rate of 0.01 Vs^{-1}. (c) Differential UV–Vis–NIR spectra. (d) Difference absorbance at selected wavelengths showing the redox switching over five successive CV cycles. (e) EPR spectra. Inset in (b) shows the cyclic voltammogram and the potential (colored circles) at which the EPR and UV–Vis–NIR spectra were taken.

Additionally, the *kite*(**Q**)–*vase*(**SQ**) switching was also achieved through chemical reduction by treating the cavitands with one or two equivalents of cobaltocene (Cp_2Co). The UV–Vis absorption spectra of **4** (Figure 8) and **2**, **3**, and **6** (Figure S28) before and after addition of Cp_2Co match the spectra observed during the corresponding electrochemical reduction. Likewise, no change in the absorption spectrum of **5** was observed when Cp_2Co was added (Figure S28).

The measurement of the binding constants in the **SQ** state is not a trivial task. As in previous quinone-based cavitands, we calculated the binding constants in the **SQ** state using CV and SWV by correlating the potential shifts to the guest concentration.[21,33,34] We found that the binding constant of **4** for 1,4-dioxane is ~ 5 times higher in the **SQ** (K_a = 52 M^{-1}) than in the **Q** state (Figure S18). However, the binding constants measured with this approach must be asserted with caution, for instance, we were not able to determine the binding constants for the other guests with enough certainty to be reported here. This drawback was noted previously, and the binding constant in the **SQ** state were instead estimated through simulations.[33,34]

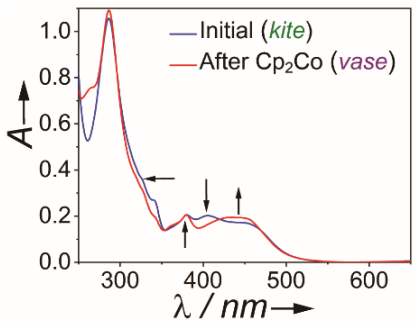

Figure 8. UV–Vis absorption of **4** before and after addition of Cp_2Co (1 x 10^{-5} M solution in deoxygenated CH_3CN saturated with Ar; 1 equiv. of Cp_2CO) at T = 298 K.

Light Activation of Resorcin[4]arene Cavitands. Having demonstrated the *kite*(**Q**)–*vase*(**SQ**) switching upon the direct chemical and electrochemical reduction of the **Q**, we investigated if the switching can be achieved by light through a photoredox process. The rationale is that upon light irradiation, the $[Ru(bpy)_2dppz]^{2+}$ wall acts as an antenna absorbing the light and then transferring one electron to the **Q** to form the **SQ**. As a secondary process, the *kite*–*vase* switching occurs once the **SQ** is generated. Therefore, the timescale of the two processes is critical for the functioning of the switch: the **SQ** must live long enough (several minutes) to be detected by EPR or UV–Vis spectroscopy and to allow for the conformational change to occur (μs–ms). If the back-electron transfer (**SQ**/Ru^{III} to **Q**/Ru^{II}) occurs in the order of ≤ μs, the *kite*–*vase* switching cannot occur and a sacrificial electron donor would be required.

The *kite*–*vase* switching upon light irradiation was monitored by UV–Vis absorption spectroscopy by comparing the spectra before and after irradiation at 420 nm. The samples were dissolved in deoxygenated solutions of CH_3CN and irradiated with a photoreactor (16 lamps, 8 W) for 15 min. Because light irradiation generates the charge-separated state (Ru^{III}/**SQ**), the UV–Vis absorption spectrum is slightly different from the one observed after chemical and electrochemical reduction (Ru^{II}/**SQ**). Nevertheless, the signature of the *vase* conformation can still be observed. In a separate experiment, EPR spectroscopy was used to confirm the formation of the **SQ**. For this purpose, the EPR spectrum in deoxygenated solutions of CH_2Cl_2 was measured during *in situ* irradiation with a visible-light LED.

Upon irradiation of cavitand **2** for 15 min in the photoreactor, no significant changes in the UV–Vis absorption spectra were observed. Likewise, **SQ** was not detected by EPR. As **2** resembles **1**, we attribute the lack of switching and the absence of the **SQ** EPR signal to the rapid back-electron transfer that competes with the slower conformational switching. Thus, the short-living **SQ** generated upon irradiation cannot be detected by steady-state techniques. Thus, we used transient absorption spectroscopy (TAS) to study the photoinduced electron transfer process of **2** and the kinetic traces upon irradiation without sacrificial electron donor are reported in the Supporting Information (Figure S29); the **SQ** was detected immediately after laser excitation indicating an intramolecular electron transfer; such early detection would not be possible during a slower diffusion-controlled intermolecular electron transfer. It was found that upon irradiation, electron transfer from the ^{3}MLCT-excited Ru^{II} to the **Q** forms the **SQ** in about 62 ns. The **SQ** has a lifetime of 6 μs before it regenerates the initial **Q**. So, in cavitand **2**, the **SQ** does not live long enough to trigger the *kite*-*vase* switching occurring at slower timescale (μs–ms). Moreover, the kinetics observed for cavitand **2** are of the same order of magnitude than the kinetics previously recorded for cavitand **1**.[36]

To accumulate the **SQ** and allow the *kite*–*vase* switching to occur in **2**, Et_3N was required as a sacrificial electron donor. Thus, when cavitand **2** was irradiated in presence of Et_3N in CH_2Cl_2 (*kite*), the UV–Vis absorption spectra displayed hypochromic shifts at 300–350 nm and 400 nm, and a hyperchromic shift at 350–400 nm (Figure S30). As similar changes in the UV–Vis absorption spectra were observed after chemical and electrochemical reduction, we confirm that the *vase* was formed upon light irradiation (Figure S30 vs Figure S28). Also, the EPR spectrum of **2** was measured during *in-situ* irradiation in presence of Et_3N and confirmed the formation of the corresponding naphthoquinone **SQ** radical anions with a septet EPR signal at *g* = 2.0048 (Figure S31).[33]

When cavitand **3**, in the *kite* conformation, was irradiated in the photoreactor for 15 min and without using Et_3N, the UV–Vis absorption spectrum showed the formation of the *vase* (Figure S30). However, no **SQ** was detected by EPR during the *in-situ* irradiation with the weaker LED (Figure S31). This can be attributed to the lower conversion yields at low-intensity irradiation. When Et_3N was added, the EPR clearly showed the formation of the naphthoquinone **SQ** with the corresponding signal at *g* = 2.0048 (Figure S31). Thus, the results indicate that the *kite*-*vase* switching in cavitand **3** can be achieved without sacrificial electron donor only with high-intensity light, otherwise sacrificial electron donor is needed when low-intensity irradiation is used.

Remarkably, the *kite*(**Q**)–*vase*(**SQ**) switching was achieved for **4** upon irradiation with both the photoreactor and the LED without using Et_3N (Figure 9). The UV–Vis absorption spectrum after irradiation shows the characteristic spectroscopic signature of the *vase* conformation (Figure 9b), while the EPR spectrum confirms the generation of the triptycene-**SQ** with the corresponding singlet EPR signal at *g* = 2.0050 (Figure 9c).

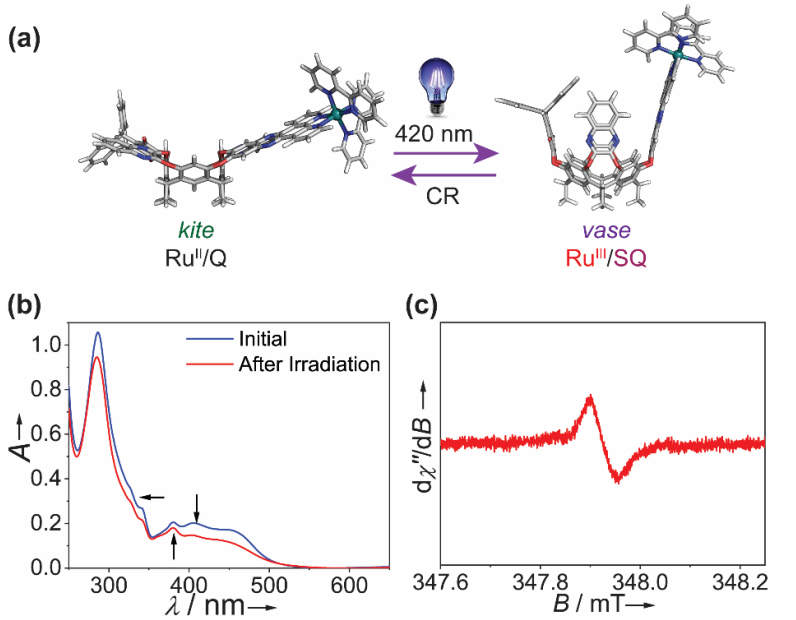

Figure 9. Light-activation of cavitand **4** in CH_3CN without sacrificial donor. (a) Schematic of the *kite-vase* switching. CR: charge recombination. (b) UV–Vis absorption spectra of **4** (1 x 10^{-5} M in CH_3CN) before and after 15 min of irradiation at 420 nm in photoreactor at T = 298 K. (c) EPR spectrum of **4** (2 x 10^{-3} M in CH_2Cl_2) after 10 min of in-situ irradiation with unfiltered light of the visible light lamp at T = 298 K.

Cavitand **4** does not require sacrificial electron donor at high- or at low-intensity light irradiation because the triptycene-quinone is a better electron acceptor (lower reduction potential) than the naphthoquinone in **3**, and the electron transfer is more efficient in **4** than in **3**. Additionally, since the distance between the **Q** and the Ru^{II}-complex is larger in **4** than in **2**, the back-electron transfer is slow enough to allow the detection of the **SQ** without sacrificial electron donor.

To investigate the decay of the **SQ** and estimate its lifetime, the EPR spectrum of **4** was measured during *in-situ* irradiation in DMF (Figures 10a–b), then the light was turned off, and the decay of the signal intensity was monitored (Figure 10c). It takes ~10 min for the **SQ** to disappear, confirming the slower back-electron transfer in **4** than in **2** (6 μs). When the light was turned on again, the **SQ** was generated almost instantaneously confirming the reversibility of the system.

As expected, irradiation of **5** and **6** did not induce changes in the UV–Vis absorption spectra or the formation of the **SQ** detected by EPR spectroscopy (Figure S30). This indicates that for light-activation of the cavitands, both components, the Ru^{II}-photosensitizer and the **Q** acceptor are required. Irradiation of only the **Q** (**6**) or the Ru^{II}-photosensitizer (**5**) at 420 nm does not generate the **SQ** or the conformational switching. Also, the lack of switching in **5** and **6** upon irradiation confirms that the conformational change observed in **2**–**4** is not triggered by a local heating effect caused by the intense light source or the non-radiative decay of the Ru^{II}-complex.

To evaluate the stability of the cavitands under the strong irradiation conditions of the photoreactor, we monitored the changes in the UV–Vis absorption spectra at different irradiation times. It was found that maximum conversion to the *vase* occurs at 15 min and decomposition starts at 20 min. Nevertheless, the *vase* conformation of **4** can be detected after 1 min of irradiation in the photoreactor. Photodecomposition can be avoided by using weaker irradiation sources than the photoreactor, although this can lead to lower formation of **SQ** and a need to use a sacrificial electron donor in certain cases. For instance, **3** required sacrificial electron donor when irradiated with a weaker lamp. This is not the case with **4**.

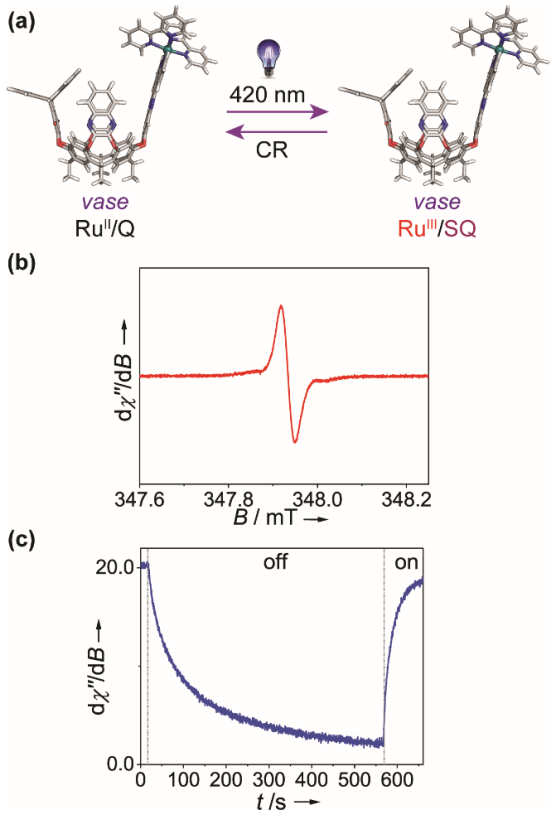

Figure 10. (a) Irradiation of **4** (*vase*) in DMF. CR: charge recombination. (b) EPR spectrum (2 x 10^{-3} M in CH_2Cl_2, T = 298 K) after 10 min of irradiation with unfiltered light of the visible light lamp. (c) Decay and rise of the **SQ** signal after turning off and on the lamp.

Table 1. Summary of switching activation of resorcin[4]arene cavitands by different stimuli.

	1	2	3	4	5	6
Conformation in						
CH_2Cl_2	*kite*	*kite*	*kite*	*kite*	*vase*	*kite*
CH_3CN	*kite*	*kite*	*kite*	*kite*	*vase*	--- [c]
DMF	*kite*	*kite*	*vase*	*vase*	*vase*	*vase*
THF	*kite*	*vase*	*kite*	*kite*	--- [c]	*vase*
Binding of guests	No	No	No	Yes	No	Yes
kite (Ru^{II}/Q) —*vase*(Ru^{II}/Q)						
Chemical and electrochemical activation	No[a]	Yes	Yes	Yes	No	Yes
kite(Ru^{II}/Q) – *vase*(Ru^{II}/SQ)						
Light activation without sacrificial donor	No	No	No[b] Yes	Yes	No	No
kite (Ru^{II}/Q) – *vase*(Ru^{III}/SQ)						
Light activation with sacrificial donor	No[a]	Yes	Yes	Yes	No	No
kite (Ru^{II}/Q) – *vase*(Ru^{II}/SQ)						

[a] Cavitand **1** can only form a partial vase upon activation. [b] Cavitand **3** can be activated with light without sacrificial donor only using a high intensity photoreactor; a lower-strength lamp does not activate **3**. [c] Cavitands are not soluble in this solvent.

Conclusion

This work presents a series of multi-stimuli responsive resorcin[4]arene cavitands designed to overcome the limitations of previously prepared light-activated cavitands: failure to form the *vase* conformation and bind smaller guests, and the need to use a sacrificial electron donor to accumulate the **SQ** and allow the *kite*–*vase* switching. Thus, the new cavitands contain different types of walls (**Q**, Qx, and Ru^{II}-based) distributed in the backbone in different configurations to tune the photoinduced electron transfer process and the ability to bind smaller guests. For instance, by varying the type, location, and number of **Q**-walls, cavitands with different gripping capabilities and with different rates of electron transfer were developed.

^{1}H NMR and UV–Vis absorption spectroscopy, DFT calculations, and crystal structures demonstrated that cavitands **2**–**6** can adopt the *vase* conformation in the **Q** state, which was not possible for previously reported cavitand **1**. Also, in contrast to cavitand **1**, cavitand **4** can encapsulate smaller guests, such as cyclohexane and related heteroalicycles in the *vase* conformation. From the new series of cavitands (**2**–**4**), higher binding constants were observed in **4** because the top of the cavity is covered by the triptycene and the ligands of the Ru^{II}-complex, which results in a slower guest exchange. EPR/UV–Vis–NIR spectroelectrochemical experiments demonstrate that the *kite*(**Q**)–*vase*(**SQ**) switching can be triggered in cavitands **2**, **3**, **4**, and **6** by electrochemical reduction of the **Q**. The same results were achieved after chemical reduction with Cp_2Co. Moreover, the switching does not occur in **5**, confirming that at least one **Q** in the backbone is indispensable for the chemical- and electrochemical-induced switching.

Visible light-activation of **4** successfully triggered the *kite*(**Q**)–*vase*(**SQ**) switching without sacrificial donor at different light intensities. However, cavitands **2** and **3** still required a sacrificial electron donor. Irradiation of cavitands **5** and **6** did not lead to any conformational change or formation of the **SQ**, demonstrating that a photosensitizing process is required and that direct photoreduction of the **Q** to form **SQ** does not occur at 420 nm. Also, the lack of conformational change upon irradiation of **5** and **6** discarded the possibility that the *kite*–*vase* switching occurs because of a local heating effect caused by the strong irradiation or the non-radiative decay of the Ru^{II}-complex.

The lessons learned in this study are summarized in Table 1. The requirements to achieve the *kite*–*vase* switching are quite clear. In contrast, the driving force for the conformational change is intriguing and, to date, only partially understood. Our data suggest that the only noticeable requirement to trigger the conformational switching to the *vase* state is the formation of at least one semiquinone radical anion wall flap. We hypothesize at this stage, that electrostatic interactions between the semiquinone radical anion and the nearby quinoxaline walls as well as solvation effects facilitate the vase formation besides possible macrocycle strain effects.[43]

The newly gained insights will pave the way to develop the next generation of light-activated molecular grippers and their implementation as sensors and nanodevices. Furthermore, the ability of cavitands **2**–**4** and **6** to be activated by multiple stimuli (host-guest interactions, solvent changes, light, and chemical and electrochemical reactions), placed them as valuable switching units that can be used to develop stimuli-responsive materials or other applications where a large molecular rearrangement and changes in the magnetic and photoluminescence properties are desired upon stimulation.

Experimental Section

Compounds **7**,**9**,**10**,**11**,**13**,**15**,**16,** and **19** were synthesized according to reported procedures.[33,36,44] The synthesis of cavitands **2**-**6** is described in detailed in the Supporting Information, which also provides characterization of the compounds, crystallographic data, binding studies, electrochemical data, and switching experiments investigated by NMR and UV-Vis spectroscopies.

Acknowledgements

The authors are grateful Dr. Bruno Bernet (ETH Zurich) for proofreading the manuscript, to Dr. Michael Solar (ETH Zurich) for his assistance performing the X-Ray crystallographic measurements, to the NMR service at ETH Zurich for their help in NMR spectroscopy, and to Klaudia Jozefjaková (STU Bratislava)

for assistance with the spectroelectrochemical experiments. MZ acknowledges the financial support of Slovak Research and Development Agency (APVV–15–0053, APVV-17-0513) and Slovak Scientific Grant Agency VEGA (1/0466/18). Work at ETH was funded by the Swiss National Science Foundation Grant 200020_159802.

Conflict of interest

The authors declare no conflict of interest

Keywords: Light-activated resorcin[4]arene cavitands • molecular grippers • ruthenium-based cavitands • semiquinone radical anion • stimuli-responsive cavitands

[1] P. L. Anelli, N. Spencer, J. F. Stoddart, *J. Am. Chem. Soc*. **1991**, *113*, 5131–5133.
[2] M. von Delius, E. M. Geertsema, D. A. Leigh, *Nat. Chem*. **2010**, *2*, 96–101.
[3] T. Kudernac, N. Ruangsupapichat, M. Parschau, M. Maciá, N. Katsonis, S. R. Harutyunyan, K.-H. Ernst, B. L. Feringa, *Nature* **2011**, *479*, 208–211.
[4] A. Coskun, M. Banaszak, R. D. Astumian, J. F. Stoddart, B. A. Grzybowski, *Chem. Soc. Rev*. **2012**, *41*, 19–30.
[5] B. Lewandowski, G. De Bo, J. W. Ward, M. Papmeyer, S. Kuschel, M. J. Aldegunde, P. M. E. Gramlich, D. Heckmann, S. M. Goldup, D. M. D'Souza, A. E. Fernandes, D. A. Leigh, *Science* **2013**, *339*, 189–193.
[6] K. Zhu, C. A. O'Keefe, V. N. Vukotic, R. W. Schurko, S. J. Loeb, *Nat. Chem*. **2015**, *7*, 514–519.
[7] C. Cheng, P. R. McGonigal, S. T. Schneebeli, H. Li, N. A. Vermeulen, C. Ke, J. F. Stoddart, *Nat. Nanotechnol*. **2015**, *10*, 547–553.
[8] S. Kassem, A. T. L. Lee, D. A. Leigh, A. Markevicius, J. Solà, *Nat. Chem.* **2016**, *8*, 138–143.
[9] B. L. Feringa, *Angew. Chem. Int. Ed.* **2017**, *56*, 11060–11078; *Angew. Chem.* **2017**, *129*, 11206-11226.
[10] V. García-López, L. B. Alemany, P.-T. Chiang, J. Sun, P.-L. Chu, A. A. Martí, J. M. Tour, *Tetrahedron* **2017**, *73*, 4864–4873.
[11] C. Pezzato, M. T. Nguyen, D. J. Kim, O. Anamimoghadam, L. Mosca, J. F. Stoddart, *Angew. Chem. Int. Ed*. **2018**, *57*, 9325–9329; *Angew. Chem.* **2018**, *130*, 9469-9473.
[12] T. Sun, G. Zhang, Q. Wang, Z. Guo, Q. Chen, X. Chen, Y. Lu, Y. Zhang, Y. Zhang, Q. Guo, X. Gao, Y. Cheng, C. Jiang, *Biomaterials* **2019**, *204*, 46–58.
[13] G. J. Simpson, V. García-López, A. D. Boese, J. M. Tour, L. Grill, *Nat. Commun*. **2019**, *10*, 4631.
[14] V. García-López, D. Liu, J. M. Tour, *Chem. Rev.* **2020**, *120*, 79–124.
[15] F.-G. Klärner, B. Kahlert, *Acc. Chem. Res*. **2003**, *36*, 919–932.
[16] I. K. Mati, S. L. Cockroft, *Chem. Soc. Rev*. **2010**, *39*, 4195–4205.
[17] K. Hermann, Y. Ruan, A. M. Hardin, C. M. Hadad, J. D. Badjić, *Chem. Soc. Rev*. **2015**, *44*, 500-514.
[18] B. Doistau, L. Benda, J.-L. Cantin, L.-M. Chamoreau, E. Ruiz, V. Marvaud, B. Hasenknopf, G. Vives, *J. Am. Chem. Soc*. **2017**, *139*, 9213–9220.
[19] C. Gropp, B. L. Quigley, F. Diederich, *J. Am. Chem. Soc*. **2018**, *140*, 2705–2717.
[20] J. V. Milić, F. Diederich, *Chem. Eur. J.* **2019**, *25*, 8440–8452.
[21] J. V. Milić, T. Schneeberger, M. Zalibera, F. Diederich, C. Boudon, L. Ruhlmann, *Electrochim. Acta* **2019**, *313*, 544–560.
[22] J. R. Moran, J. L. Ericson, E. Dalcanale, J. A. Bryant, C. B. Knobler, D. J. Cram, *J. Am. Chem. Soc*. **1991**, *113*, 5707–5714.
[23] V. A. Azov, B. Jaun, F. Diederich, *Helv. Chim. Acta* **2004**, *87*, 449–462.
[24] J. R. Moran, S. Karbach, D. J. Cram, *J. Am. Chem. Soc.* **1982**, *104*, 5826–5828.
[25] L. M. Tunstad, J. A. Tucker, E. Dalcanale, J. Weiser, J. A. Bryant, J. C. Sherman, R. C. Helgeson, C. B. Knobler, D. J. Cram, *J. Org. Chem*. **1989**, *54*, 1305–1312.
[26] D. J. Cram, J. M. Cram, *Container Molecules and Their Guests*, Royal Society of Chemistry, Cambridge, 1994.
[27] P. J. Skinner, A. G. Cheetham, A. Beeby, V. Gramlich, F. Diederich, *Helv. Chim. Acta* **2001**, *84*, 2146–2153.
[28] P. Roncucci, L. Pirondini, G. Paderni, C. Massera, E. Dalcanale, V. A. Azov, F. Diederich, *Chem. Eur. J.* **2006**, *12*, 4775–4784.
[29] I. Pochorovski, C. Boudon, J.-P. Gisselbrecht, M.-O. Ebert, W. B. Schweizer, F. Diederich, *Angew. Chem. Int. Ed*. **2012**, *51*, 262–266; *Angew. Chem.* **2012**, *124*, 269-273.
[30] M. Frei, F. Marotti, F. Diederich, *Chem. Commun*. **2004**, 1362–1363.
[31] I. Pochorovski, J. Milić, D. Kolarski, C. Gropp, W. B. Schweizer, F. Diederich, *J. Am. Chem. Soc*. **2014**, *136*, 3852–3858.
[32] O. B. Berryman, A. C. Sather, J. Rebek, Jr., *Chem. Commun*. **2011**, *47*, 656–658.
[33] J. Milić, M. Zalibera, I. Pochorovski, N. Trapp, J. Nomrowski, D. Neshchadin, L. Ruhlmann, C. Boudon, O. S. Wenger, A. Savitsky, W. Lubitz, G. Gescheidt, F. Diederich, *J. Phys. Chem. Lett.* **2016**, *7*, 2470-2477.
[34] J. Milić, M. Zalibera, D. Talaat, J. Nomrowski, N. Trapp, L. Ruhlmann, C. Boudon, O. S. Wenger, A. Savitsky, W. Lubitz, F. Diederich, *Chem. Eur. J.* **2018**, *24*, 1431–1440.
[35] Y. Pellegrin, F. Odobel, *C. R. Chimie* **2017**, *20*, 283–295.
[36] V. García-López, J. V. Milić, M. Zalibera, D. Neshchadin, M. Kuss-Petermann, L. Ruhlmann, J. Nomrowski, N. Trapp, C. Boudon, G. Gescheidt, O. S. Wenger, F. Diederich, *Tetrahedron* **2018**, *74*, 5615–5626.
[37] I. Pochorovski, F. Diederich, *Acc. Chem. Res*. **2014**, *47*, 2096−2105.
[38] Gaussian 09 (Revision D.01), M. J. Frisch, G. W. Trucks, H. B. Schlegel, G. E. Scuseria, M. A. Robb, J. R. Cheeseman, G. Scalmani, V. Barone, B. Mennucci, G. A. Petersson, H. Nakatsuji, M. Caricato, X. Li, H. P. Hratchian, A. F. Izmaylov, J. Bloino, G. Zheng, J. L. Sonnenberg, M. Hada, M. Ehara, K. Toyota, R. Fukuda, J. Hasegawa, M. Ishida, T. Nakajima, Y. Honda, O. Kitao, H. Nakai, T. Vreven, J. A. Montgomery, Jr., J. E. Peralta, F. Ogliaro, M. Bearpark, J. J. Heyd, E. Brothers, K. N. Kudin, V. N. Staroverov, R. Kobayashi, J. Normand, K. Raghavachari, A. Rendell, J. C. Burant, S. S. Iyengar, J. Tomasi, M. Cossi, N. Rega, J. M. Millam, M. Klene, J. E. Knox, J. B. Cross, V. Bakken, C. Adamo, J. Jaramillo, R. Gomperts, R. E. Stratmann, O. Yazyev, A. J. Austin, R. Cammi, C. Pomelli, J. W. Ochterski, R. L. Martin, K. Morokuma, V. G. Zakrzewski, G. A. Voth, P. Salvador, J. J. Dannenberg, S. Dapprich, A. D. Daniels, Ö. Farkas, J. B. Foresman, J. V. Ortiz, J. Cioslowski, D. J. Fox, Gaussian, Inc., Wallingford CT, **2009**.
[39] P. J. Hay, W. R. Wadt, *J. Chem. Phys.* **1985**, *82*, 270–283.
[40] W. R. Wadt, P. J. Hay, *J. Chem. Phys.* **1985**, *82*, 284–298.
[41] J. Fees, W. Kaim, M. Moscherosch, W. Matheis, J. Klíma, M. Krejčík, S. Záliš, *Inorg. Chem*. **1993**, *32*, 166–174.
[42] R. Calvo, E. C. Abresch, R. Bittl, G. Feher, W. Hofbauer, R. A. Isaacson, W. Lubitz, M. Y. Okamura, M. L. Paddock, *J. Am. Chem. Soc*. **2000**, *122*, 7327–7341.
[43] D. F. Hahn, J. V. Milić, P. H Hünenberger, *Helv. Chim. Acta* **2019**, *102*, e1900060).
[44] P. P. Castro, G. Zhao, G. A. Masangkay, C. Hernandez, L. M. Gutierrez-Tunstad, *Org. Lett*. **2004**, *6*, 333-336.

Entry for the Table of Contents

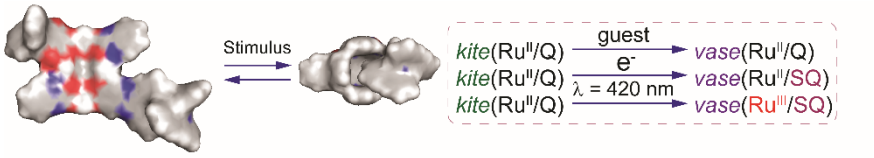

Resorcin[4]arene cavitands functionalized with an electron-accepting quinone and a $[Ru(bpy)_2dppz]^{2+}$ photosensitizing wall can be switched upon visible light irradiation between a flat *kite* in the quinone state **Q** and a *vase* conformation in the semiquinone radical anion state **SQ**. At optimal molecular design, photoredox switching occurs without addition of a sacrificial donor. Conformational switching can also be triggered by changes in solvent, host-guest interactions, and chemical and electrochemical processes.